2023

A Numerical Analysis of Shock Angles from Inward Turning Axisymmetric Flows

William L. Hilal
University of Central Florida

A NUMERICAL ANALYSIS OF SHOCK ANGLES FROM INWARD-TURNING AXISYMMETRIC FLOWS

by

WILLIAM L. HILAL

A thesis submitted in partial fulfillment of the requirements
for the Honors in the Major Program in Aerospace Engineering
in the College of Engineering and Computer Science
at the University of Central Florida
Orlando, Florida

Spring Term, 2023

Thesis Chair: Kareem Ahmed, Ph.D.

ABSTRACT

Detonation-based propulsion systems are known for their high efficiency and energy release when compared to deflagrative systems, making them an ideal candidate in hypersonic propulsion applications. One such engine is the Oblique Detonation Wave (ODW) engine, which has a similar architecture to traditional scramjets but shortens the combustor and isolator to an anchored ODW after fuel injection.

Previous research has focused on using a two-dimensional wedge to induce an ODW while limiting total losses through the combustor. In this configuration, a two-dimensional wedge-based architecture entails a rectangular duct, limiting potential inlet design and increasing overall skin friction. However, an inward-turning axisymmetric ODW wedge architecture, where a two-dimensional wedge is revolved around a central axis, has yet to be examined in detail. The work at present aims to investigate the fundamental physics required to predict the Oblique Shock Wave (OSW) for an inward-turning axisymmetric flow, which is critical for designing a circular ODW engine combustor. Multiple steady simulations of inviscid and ideal air at Mach 4, 6, and 8 were performed over a 1-inch wedge with wedge angles of 16°, 18°, and 20°. The radius of the inlet boundary was also varied between 1, 3, and 5 inches to examine the effect of increasing the blockage ratio.

The results showed that the shock angle for an inward-turning axisymmetric flow was up to 8% steeper than the analytical, two-dimensional wedge solution. Additionally, it was found that the OSW diverged further from the two-dimensional solution when the blockage ratio was increased. These findings provide insight into the flow physics that must be considered when designing inward-turning axisymmetric ODW engines.

ACKNOWLEDGEMENTS

The author would like to acknowledge the UCF Propulsion & Energy Research Laboratory (PERL) and Dr. Kareem Ahmed for providing the opportunity to conduct this research. Additionally, the author would like to acknowledge the UCF Hypersonics team for their continued support and knowledge, namely Austin Burden, Adam Kotler, Mason Thornton, Zachary White, Justin Sprunger, and Robyn Cideme.

TABLE OF CONTENTS

LIST OF FIGURES

CHAPTER 1: BACKGROUND

A detonation wave is a pressure-coupled supersonic combustion wave in which the ignition of incoming reactants occurs from adiabatic heating generated by a leading shock wave. In other words, a supersonic combustion wave across which thermodynamic states (e.g., pressure and temperature) increase sharply is known as a detonation [1]. By contrast, deflagrations are characterized by an uncoupled shock front followed by a spatially distinct combustion front [2]. As such, detonations realize a self-induced rapid chemical conversion, typically on the order of magnitude of tens of thousands of times faster when compared to deflagrative burning, allowing detonation-based combustors to be much higher performing than their deflagrative-based counterparts [3]. Detonations are thermodynamically represented as an isochoric process due to the small-time scale between reactant dissociation and combustion, whereas deflagrative burning is treated as a constant pressure process [4]. This phenomenon is known as pressure-gain combustion, allowing detonations to operate at considerably higher thermodynamic efficiencies (~10-20%) [3]. As such, considerable interest has been placed on using detonations to lead the next generation of hypersonic propulsion engines.

An engine of particular interest is the Oblique Detonation Wave Engine (ODWE). ODWEs utilize a standing Oblique Detonation Wave (ODW), which is a combustion-inducing Oblique Shock Wave (OSW), to combust incoming propellants [5]. An ODW is formed when an OSW and subsequent deflagration waves merge into a single, resolvable structure [6]. The architecture of a typical ODWE most closely resembles that of a scramjet, where the combustor and isolator are shortened to an anchored ODW after fuel injection and adequate mixing [7]. Various analyses have

demonstrated satisfactory ODWE performance in freestream Mach numbers ranging from 7 – 20 [8]–[11]. Ashford et al. compared ODWE and diffusive scramjet performance for a range of freestream Mach numbers, fuel flow rates (H_2,CH_4), altitudes, and various inlet conditions. It was found that an ODWE demonstrates comparable performance to a diffusive scramjet engine while producing less drag and less engine heat transfer from a smaller longitudinal profile [8]. As such, it is widely assumed that ODWE performance supersedes that of a scramjet as flight at and above Mach 12 is achieved [12]. These findings have prompted further analytical [2], experimental [12]–[16], and computational work [9], [16]–[20] into ODWE formation and stabilization to expand its development.

ODWE research has been primarily focused on the use of a two-dimensional (2D) wedge-induced ODW because total realized pressure losses are significantly less across an OSW than that of a partial normal shock wave produced by a blunt body [13]. Additionally, a wedge minimally penetrates into the freestream, allowing for significantly less adverse pressure drag effects in hypersonic environments. Li. et al. numerically investigated the structure of wedge-induced detonations, concluding the detonation structure consisted of the following elements: (1) a non-reactive OSW, (2) an induction zone, (3) a set of deflagration waves, and (4) a close-coupled "reactive shock" with heat release (ODW), shown in Figure 1 [6].

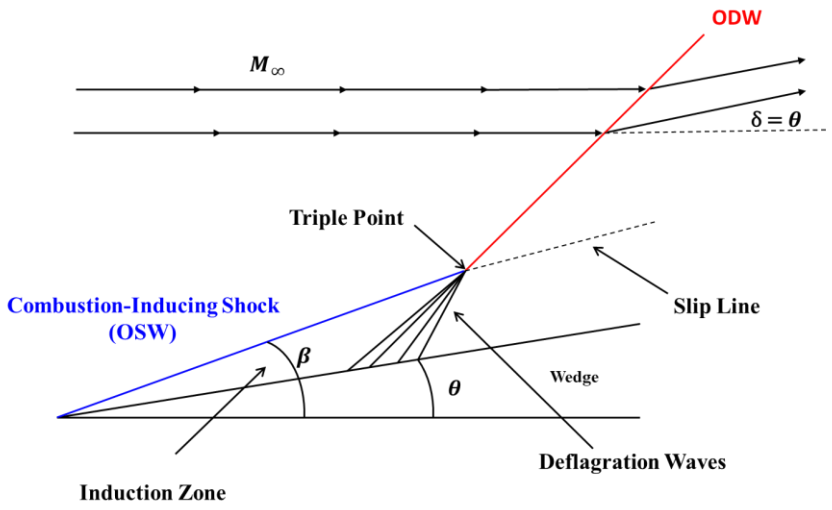

Figure 1: Wedge-Induced Detonation Structure

Before a wedge-induced ODW stability band can be discussed in detail, it is important to establish a general understanding of OSW phenomena over a wedge. OSWs can exist within a β range of $\sin^{-1}\left(\frac{1}{M}\right) \leq \beta \leq \frac{\pi}{2}$, where the upper-limiting case is that of a normal shock [14]. Equation 1 shows a relationship between turning angle and the resulting wave angle of the shock for an infinite wedge, where M is the freestream Mach number, β is the wave angle, γ is the ratio of specific heats, and θ is the flow turning angle.

$$tan(\theta) = 2\,cot\,\beta\,(\frac{M^2\,sin^2\,\beta - 1}{M^2[\gamma + cos(2\beta)] + 2}) \tag{1}$$

This equation can be numerically solved for β to yield any shock angle for a given turning angle, Mach number, and ratio of specific heats. Plotting all numerical solutions and assuming a constant γ of 1.4 yields a solution set shown in Figure 2. It should be noted that Equation 1 yields both a weak and strong shock solution for the same turning angle and Mach number. However, only the weak solution will occur in supersonic flow at near-atmospheric conditions [14]. Thus, only the

weak solution will be considered limiting the stability band for an OSW to $\sin^{-1}\left(\frac{1}{M}\right) \leq \beta \leq \beta_{max}$ where β_{max} is the maximum shock angle prior to the OSW detaching.

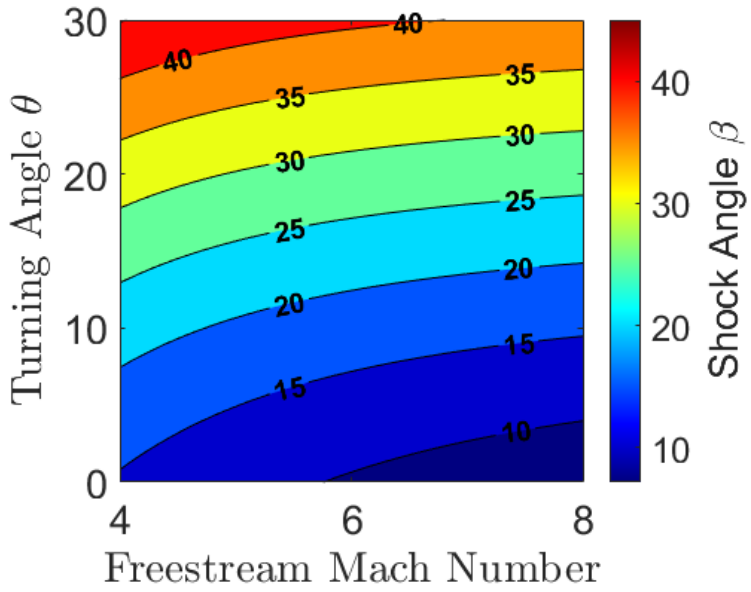

Figure 2: Shock Angle (β) as a Function of Freestream Mach Number and Turning Angle (θ) in Ideal, Inviscid Air with γ = 1.4

An OSW will detach when certain flow field parameters are unable to be met by an attached shock, namely continuity and conservation of momentum [14]. The detached shock then becomes a bow shock that resides upstream of the turning geometry. The shape of the wave and detachment distance are functions of both Mach number and geometry [14]. To find the turning angles that will cause the OSW to detach, θ_{max} , the derivative of Equation 2 must be taken. The derivative can then be set to zero and rearranged, yielding an expression that can be solved for maximum shock angles, β_{max}. This is shown in Equation 3. The corresponding maximum turning angle can be then determined from Equation 1. The value for which flow separation occurs for a given turning angle and Mach number is shown in Figure 3. Figures 2 and 3 taken together outline the

stability band for an OSW in inviscid, ideal air at a freestream of Mach numbers 4 through 8 being turned by an infinite, 2D wedge. Additionally, these values assume a constant γ of 1.4. It should be mentioned here that large shock angles are not practical for ODWE configurations due to significant pressure losses realized by steepening the shock closer to normal. However, this information is still provided to give insight into the range of plausible turning angles that can be considered for ODW architectures. This information taken holistically is necessary to establish a general regime of ODW stability, which will be discussed next.

$$cot(\theta) = tan(\beta)\left[\left(\frac{\gamma+1}{2}\right)\frac{M^2}{M_1^2\, sin^2\,\theta - 1} - 1\right] \tag{2}$$

$$sin^2\,\beta_{max} = \frac{1}{\gamma M^2}\{\left(\frac{\gamma+1}{4}\right)M^2 - 1 + \sqrt{(\gamma+1)[\frac{(\gamma-1)}{16}M^4 + (\frac{\gamma-1}{2})M^2 + 1]}\ \} \tag{3}$$

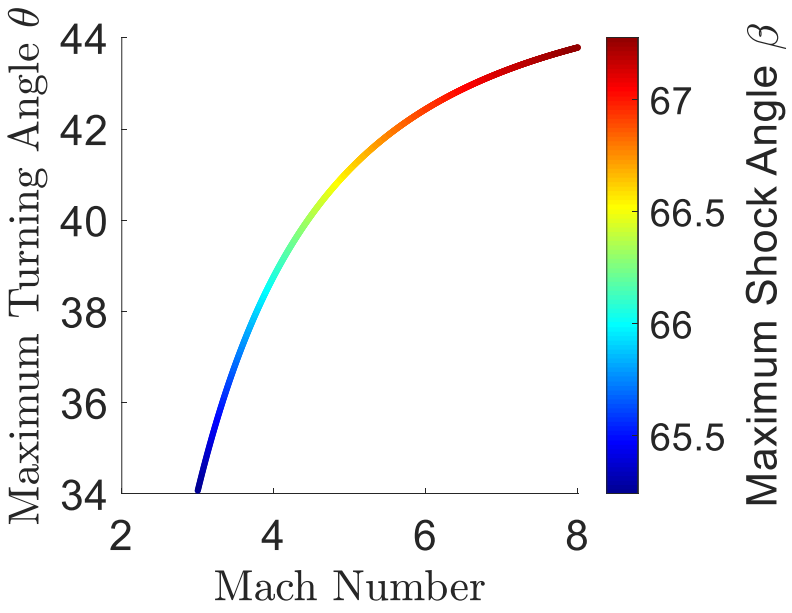

Figure 3: Maximum Shock Angle as a Function of Freestream Mach Number and Maximum Turning Angle in Ideal, Inviscid Air with $\gamma = 1.4$

An early numerical study conducted by Li et al. addressed the formation process of an ODW over a wedge through a numerical model and found that the simulated ODW was stable in a wide range of flow and mixture conditions [6]. Pratt et al. determined a general stability band using oblique shock polars for a wedge-based ODWE with chemical heat release where a nondimensional heat release was defined as $\tilde{Q} = \frac{Q}{C_p T}$ [2]. Here, Q is the heat release, C_p is the constant pressure heat capacity and T is the inflow static temperature. A value for $\tilde{Q}$ is typically determined for a chemical mixture through a combustion reaction model at a specific operating temperature and pressure. The Chapman-Jouget (CJ) Mach number (M_{CJ}) is the minimum value at which a self-sustaining detonation with a supersonic condition behind it can propagate through a combustible mixture of gases [1]. M_{CJ} for an ODW can be calculated as a function of the nondimensional heat release, $\tilde{Q}$, and the ratio of specific heats, γ. This is shown in Equation 4. It should be noted that M_{CJ} is defined as the normal component to the ODW, not the freestream Mach number. The CJ wave angle, β_{CJ}, is the shock angle corresponding to the CJ Mach Number, M_{CJ}. β_{CJ} is defined such that the normal component of the inflow to the OSW is M_{CJ}, shown in Equation 5 where M is the freestream Mach number. Lastly, a CJ turning angle, θ_{CJ}, is defined as a function of β_{CJ}, M_{CJ}, and γ.

$$M_{CJ}^2 = \left[1 + \tilde{Q}(\gamma + 1)\right] + \sqrt{\left[1 + \tilde{Q}(\gamma + 1)\right]^2 - 1} \tag{4}$$

$$\beta_{CJ} = sin^{-1}\left(\frac{M_{CJ}}{M}\right) \tag{5}$$

$$\theta_{CJ} = \beta_{CJ} - tan^{-1}\left(\frac{1 + \gamma M_{CJ}^2}{(\gamma + 1)M_{CJ}^2\sqrt{\left(\frac{M}{M_{CJ}}\right)^2 - 1}}\right) \tag{6}$$

θ_{CJ} represents the minimum turning angle for which a stable heat release can occur for a given freestream Mach number and $\tilde{Q}$ [2]. This bounds the lower limit of attached ODW turning angles to θ_{CJ} [2]. Importantly, θ_{CJ} corresponds to the point of minimum entropy production as the normal component of the freestream Mach number is at unity across the shock. Thus, ODW architectures are ideally designed to operate near a detonation's CJ condition [15]. Because θ_{CJ} is largely dependent on the location of the OSW, β, it is very important to first characterize β in any flow path for which an ODWE is being considered. For future wedge-based ODW architectures, as considered in this paper, characterizing the stability range of the OSW is of vital importance.

Furthermore, a reactive shock polar analysis conducted by Pratt et al. demonstrated that the turning angle at which the ODW becomes detached from the leading edge is the same as adiabatic, OSW detachment [2]. This bounds θ_{max} for an ODW to the maximum turning angle of a similar OSW case. Figure 2 displays the theoretical upper and lower limits of ODW stability for a reacting hydrogen-air mixture at 500 K.

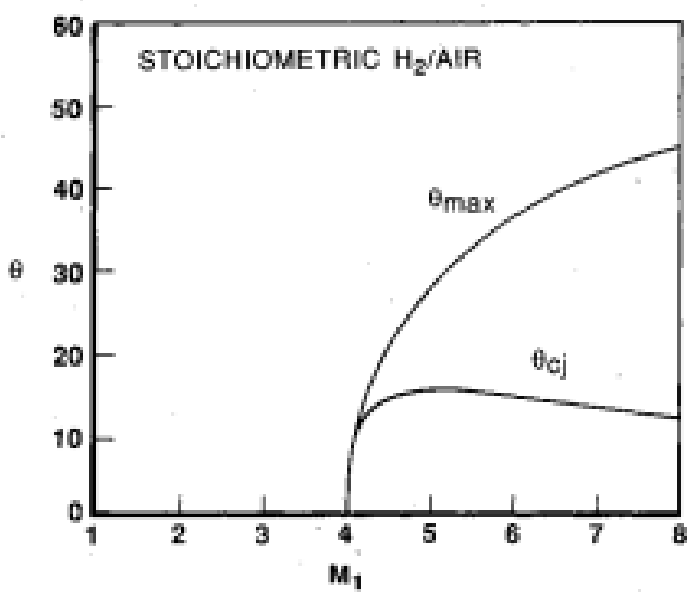

Figure 4: Stoichiometric Hydrogen-Air ODW Stability Limits at 500 K [2], [7]

As discussed above, a minimum OSW for a given freestream Mach number can only exist at $\sin^{-1}\left(\frac{1}{M}\right)$ to satisfy the second law of thermodynamics [14]. Comparing θ_{CJ} to the minimum OSW angle at each Mach number shown in Figure 1, it is clear that $\tilde{Q}$ drives the ODW steeper in space, reducing the permitted range of attached ODWs. This was mentioned by Li et al. who observed that the shock structure in front of the induction zone was governed by the OSW relations, but the ODW reorients itself to a steeper angle above the induction zone to accommodate both heat release and flow turning [6]. This can be generalized in ODW shock polars, which consider heat release to establish a general regime of ODW stability. Figure 5 demonstrates the generalized ODW angle as a function of turning angle and $\tilde{Q}$. The region of interest for propulsive application is bounded by the lower θ_{CJ} and the upper OSW detachment angle, known as a weak overdriven detonation wave [5].

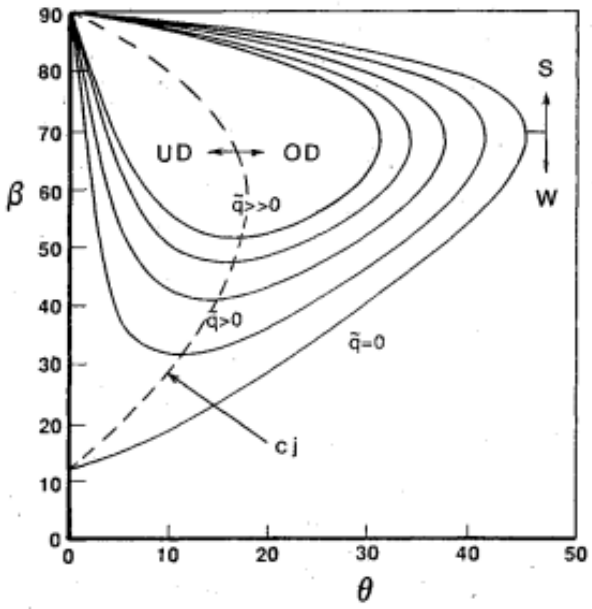

Figure 5: Turning Angles versus ODW Angle with $\widetilde{Q}$ [2]

Extensive experimental and numerical work has been done to characterize the stability and formation of an ODW over a finite wedge. Lu et al. numerically modeled a detonation on a two-dimensional wedge in a premixed hydrogen-air freestream [16]. Turning angle and incoming Mach number varied, resulting in the observation of both up-stream propagating detonation waves and standing detonation waves. Xiang et al. conducted a 2D numerical analysis on the interactions between two ODWs induced by symmetric finite wedges in a hydrogen-air freestream. The resulting flow features were characterized including a Mach stem, reflected detonation waves, and slip lines. [17]. Xiang et al. also varied the inlet size, observing that the ODW Mach stem increased in length as the inlet length increased. Teng et al. evaluated the effect of stagnation pressure and Mach number on ODW initiation over a finite wedge in a pre-mixed hydrogen-air freestream [18]. Fusina presented a novel ODWE design that stabilized an ODW over wedge-shaped flame holders in a steady, two-dimensional hydrogen-air numerical model [19]. Additionally, Fusina et al.

conducted a time-accurate, numerical simulation on the formation of ODWs on an inviscid wedge near their CJ condition [20]. A 1- and 0.1-μs time step indicated that the ODW reached a non-oscillatory position in the laminar, two-dimensional regime [21]. To address the lack of inviscid simulations, Fang. et al. considered a viscous, 2D, and semi-infinite wedge with an inflow of Mach 7 and 10, finding that the boundary layer formed on the wedge has a non-negligible effect on ODW position [22]. Bachman et al. performed a high-fidelity, viscous numerical simulation of an ODW anchored to a 4 cm wedge in a 9 cm inflow flow field. A Mach 5 flow was considered with static temperatures of 600 K, 700 K, and 800 K. A quasi-stable ODW was observed, stemming from the interaction between the boundary layer and the ODW [7]. Bachman et al. further examined a double-angle, 2D wedge that transitioned from 11 degrees to 12.5 degrees at 2 inches to attempt to stabilize a detonation in a pre-mixed, viscous hydrogen-air freestream. A Mach 5 freestream at both 700 K and 800 K were explored, finding that the boundary layer augmented the flow turning angle to within ODW stability limits to form a stable ODW despite $\theta < \theta_{CJ}$ [23]. Rosato et al. conducted experimental testing of a 30-degree wedge in a Mach 4.4 freestream, near the maximum of the analytical ODW stability shock polar at the given flow conditions. An ODW was experimentally stabilized, marking a major milestone in the development of standing detonation engines. More experimental testing was subsequently conducted in the same facility to experimentally examine the viability of the ODW stability band closer to the θ_{CJ}. Thornton et al. extended the work of Rosato et al. in the same high-enthalpy facility with a 12-degree and 20-degree wedge in addition to a 30-degree wedge. The 30-degree wedge yielded a quasi-stable ODW, while the 12- and 20-degree wedges did not [24]. Research at present is focused on further expanding the experimental data of a 2D wedge-induced ODW to provide more insight into the flight capabilities of an ODWE.

However, a limiting downside to a 2D wedge-based ODWE architecture is that it entails a rectangular duct, limiting potential ODWE inlet design and increasing overall skin friction throughout the engine. An extension of wedge-induced ODW research that has yet to be explored is the potential architecture of rotating the wedge around a center axis. The present work investigates the flow features, namely the OSW location, generated from rotating a 2D finite wedge around a center axis in a numerical domain to model the flow path of a theoretical ODWE combustor. This work will extend existing ODW research by helping lay the foundational knowledge required to design and conduct inward-turning ODWE testing more accurately. This knowledge will be critical in determining the ODW stability parameters needed to design the next generation of ODWE combustors.

CHAPTER 2: NUMERICAL MODEL AND PROCEDURE

Two computational domains were examined in the work at present: a 2D wedge and an inward-turning axisymmetric wedge. The 2D wedge was modeled using a parametric design that included a wedge penetrating a freestream at a fixed angle. The wedge for both cases was set to a constant length of 1 inch, which is similar to the wedge lengths in existing ODW literature [17], [21], [23]–[25]. The initial conditions specified a fully developed flow at a certain Mach number. Air was used as the working fluid, and the ratio of specific heats was held constant at γ =1.4. The fluid domain was inviscid, ideal, and steady. A 1-inch pre-wedge and a 5-inch post-wedge distance were added to the computational domains to allow the flow features to fully develop. In the computational space, 16, 18, and 20-degree wedges were examined at Mach numbers 4, 6, and 8. The inlet static pressure and static temperature were set at 10 psi and 300 K, respectively. It should be noted that Equation 1 indicates no dependence on inlet pressure or temperature for analytical OSW position. Thus, the inlet static temperature and pressure are set as a formality which were held constant between all computational cases.

Additionally, inlet lengths of 1, 3, and 5 inches were examined for the 2D wedge. This allowed for an investigation between the normalized penetration of the wedge into the freestream and the resulting shock angle. The computational space can be seen in Figure 6, where the negative space of a wedge is modeled and each of the parameters of interest are listed. Furthermore, Mach numbers, turning angles, and inlet sizes were all chosen as such based on similarity to previous numerical and computational ODW studies [17], [21], [23]–[25]. All numerical modeling was carried out using STAR-CCM+, a computational fluid dynamics simulation (CFD) solver.

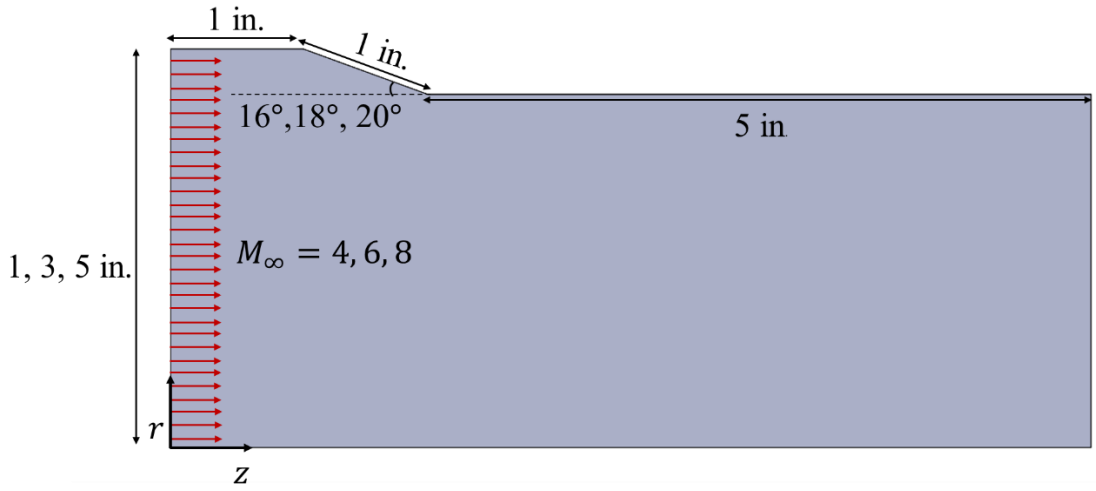

Figure 6: Computational Domain of Two-Dimensional Wedge

Assuming a steady, inviscid, and compressible flow simplifies the Navier-Stokes equations to the equations shown below. The ideal gas equation of state was used in tandem to numerically solve the fluid field in full. Shown below are the continuity, momentum, and energy equations which governed the 2D fluid regime for all two-dimensional wedge simulations.

$$\int_A \rho \boldsymbol{v} \cdot d\boldsymbol{a} = 0 \tag{7}$$

$$\oint_A \rho \mathbf{v} \otimes \mathbf{v} \cdot \mathrm{d}\mathbf{a} = \oint_A P\boldsymbol{I} \cdot \mathrm{d}\mathbf{a} \tag{8}$$

$$\oint_A \rho H \mathbf{v} \cdot \mathrm{d}\mathbf{a} = -\oint_A \boldsymbol{q} \cdot \mathrm{d}\mathbf{a} \tag{9}$$

$$\boldsymbol{\rho} = \frac{\mathrm{p}}{\mathrm{RT}} \tag{10}$$

In the above equations, ρ is the density, **a** is the area vector, **v** is the velocity, P is the pressure, H is the total enthalpy, $\boldsymbol{q}$ is the heat flux, and $\otimes$ is the tensor product. Importantly, R = $\frac{R_u}{M}$ where R_U is the universal gas constant 8.31446 J/mol K.

The equations above are coupled differential equations and must be solved simultaneously with the equation of state. The velocity field in the domain was resolved using the momentum equations. The pressure was calculated from the continuity equation and the density was evaluated from the equation of state. Because the solution was steady, or quasi-steady, a coupled implicit solver was used to solve the coupled flow. The base mesh size was set to 60 micrometers, with mesh refinement around the OSW as low as 2 micrometers. This was done to balance the computational times with shock resolution as all predicted models were correct within .25% of the analytical solution. An automatic CFL control method was used to best optimize converge time by automatically adjusting in response to the algebraic-multi-grid solver.

The OSW that formed off each wedge was captured using multiple line probes that detected a rapid change in Mach number and static pressure. The cell location of this occurrence was recorded in two locations: 75% of the height of the wedge and at the height of the wedge, as shown in Figure 7. By fixing the y-axis offset between the probes, Equation 11 was then used to determine the resulting shock angle in each simulation. Each line probe had a resolution of 100,000 and a length of .7 inches, making the step size an order of magnitude less than the minimum cell size.

$$\beta = atan\left(\frac{dr}{dz}\right) \tag{11}$$

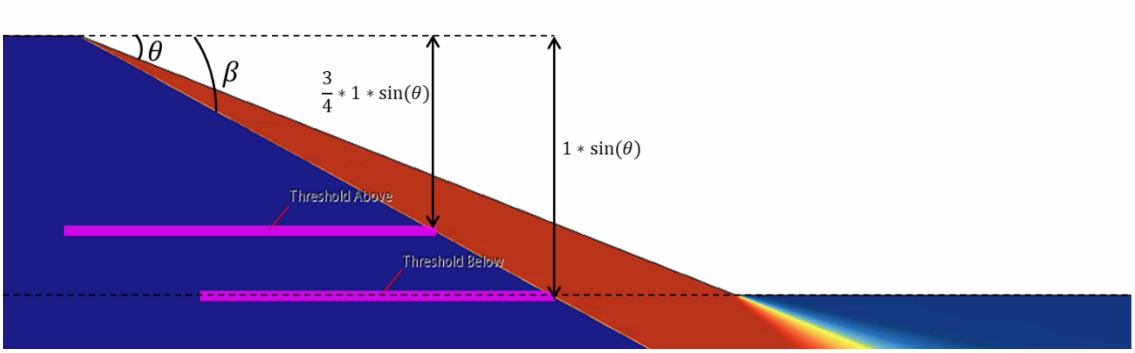

Figure 7: Computational Domain with Line Probes to Detect Shock Location

The inward-turning, axisymmetric flow was modeled on a 2D solution domain to shorten computational times. This required that the bottom boundary in Figure 6 be set to a rotational axis within the solver. A 1-inch wedge, 1 inch pre-wedge distance and a 5-inch post-wedge were held constant for consistency between simulations. The conservation equations of mass and energy remained the same as the 2D case, shown by Equations 7 and 9. The momentum equation for the axisymmetric case is shown in Equation 12. The momentum equation was represented without swirl because the freestream was inviscid and irrotational. Additionally, the circumferential velocity and the circumferential gradients were zero as the flow was inviscid. Equation 12 was then numerically solved for the inviscid, ideal, and steady flow of all axisymmetric cases.

$$\oint_{dA} \rho \mathbf{v} \otimes \mathbf{v} \cdot r ds = -\oint_{dA} P\boldsymbol{I} \cdot r ds \tag{12}$$

In Equation 12, A is the area, dA is the contour of A, $\boldsymbol{I}$ is the identity matrix, and $\mathbf{v}$ is velocity. Like the 2D cases, the r direction is the radial direction of the flow outward from the axis of rotation and the direction of the freestream is z. A cutaway of the computational domain as viewed by the coupled solver is shown in Figure 8 where the rotational axis is introduced.

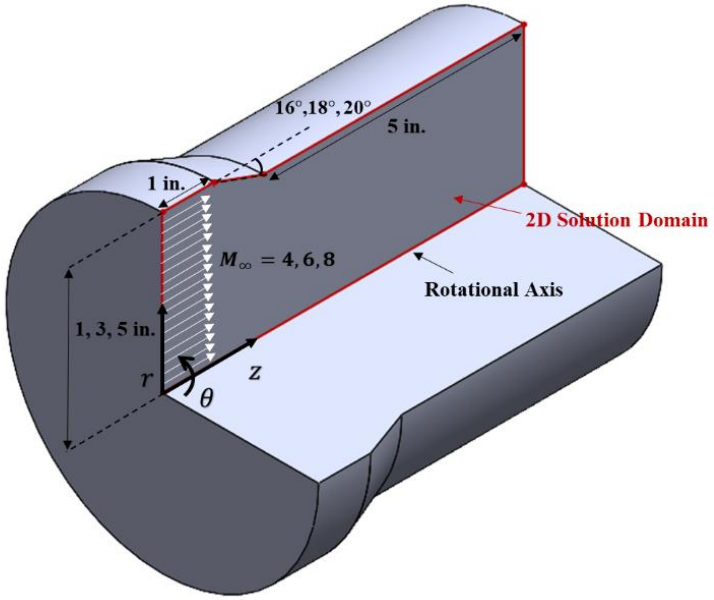

Figure 8: Computational Domain of Inward-Turning Axisymmetric Wedge

The numerical test matrix for the inward-turning axisymmetric simulations was the same as discussed for the non-axisymmetric case in which Mach 4, 6, and 8 were set as inlet conditions over 16, 18, and 20 degree-turning angles before changing the inlet radii and repeating. The grid size and method of determining OSW angle were also held constant for consistency between simulations. The OSW location was measured the same way for the axisymmetric cases as it was for the 2D cases. The difference in OSW location between the 2D and axisymmetric cases was then compared for each case with similar flow physics.

The ratio of flow area before and after the wedge was also considered to determine if there was any impact on OSW location as in the inlet area was increased in size for both flow domains. This relationship will be referred to as the "blockage ratio" and can be analytically calculated by determining the restriction of the flow area, as shown in Figures 9 and 10. For the 2D and axisymmetric cases, the blockage ratio can be expressed mathematically as $\frac{L_2}{L_{Inlet}}$ and $\frac{A_2}{A_{Inlet}}$,

respectively. An important expression used to quantify the effect of the blockage ratio is defined as the percent difference of β. This expression is defined in Equation 13 and will be a key parameter in normalizing the differences between the OSW angles across different test cases.

$$\%Difference_{\beta} = \frac{\beta_{analytical} - \beta_{observed}}{\beta_{observed}} \tag{13}$$

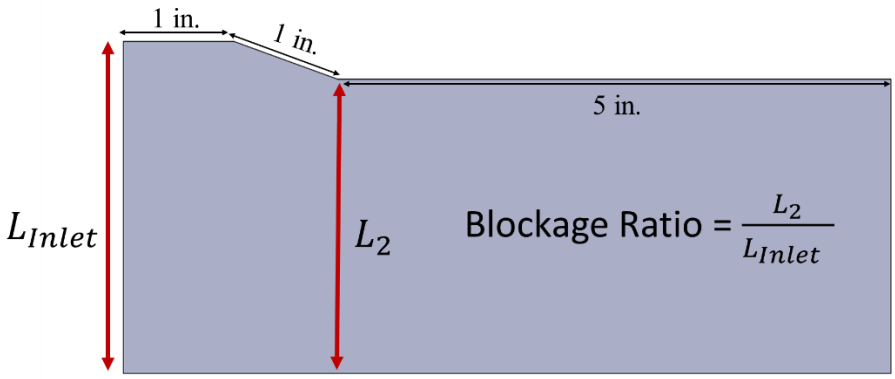

Figure 9: Blockage Ratio of the Two-Dimensional Wedge Domain

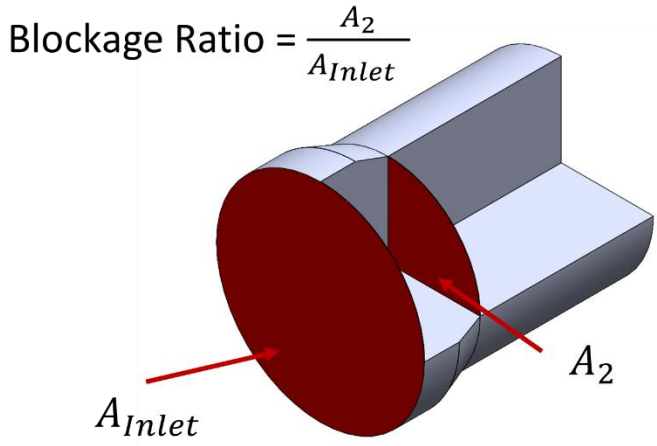

Figure 10: Blockage Ratio of the Inward-Turning Axisymmetric Wedge Domain

CHAPTER 3: RESULTS

Two-Dimensional Wedge Domain

To begin, it was first important to validate that the solver was matching the analytical solutions for an ideal flow of supersonic Air with a constant $\gamma = 1.4$ for the flow-paths under examination. A scalar representation of a fully resolved, numerical domain is also provided in Figure 11 for a 2D wedge model. The OSW is seen reflecting off the bottom axis and subsequently forming an oblique shock train to the exit of the flow path. All flow features are consistent with known supersonic, inviscid, ideal flow through a 2D channel. Figure 12 displays the findings from the numerical model plotted alongside the analytical solutions for the OSW standing wave position for the three different wedge angles. The analytical solutions were generated using Equation 1 and are displayed as colored lines.

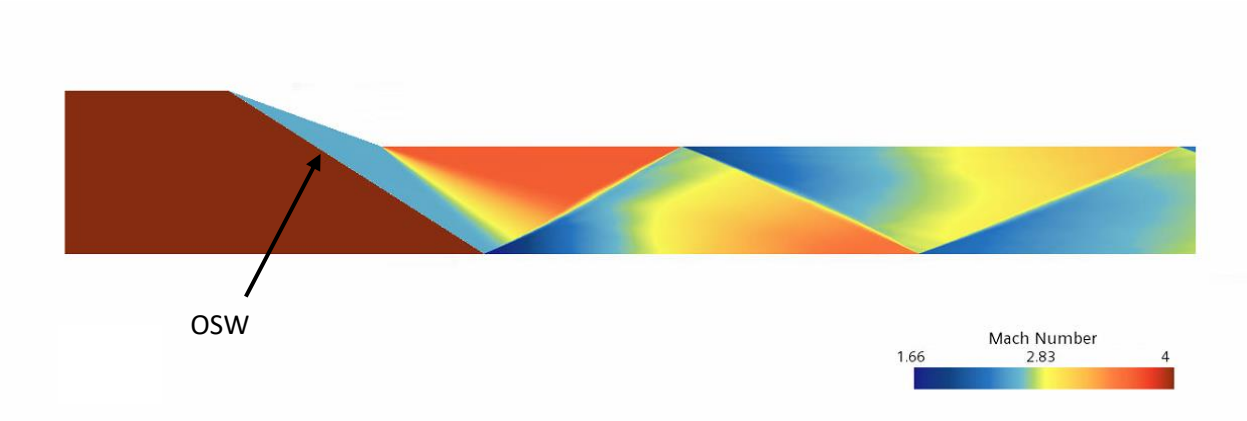

Figure 11: Mach Scalar of Numerical Two-Dimensional Wedge Model with a 1 Inch Inlet and $\theta = 20°$

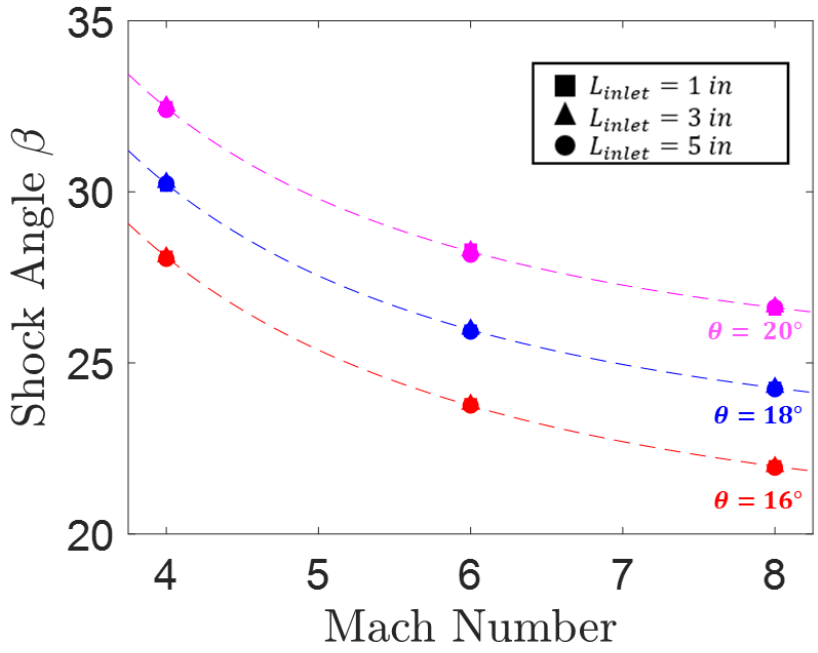

Figure 12: Mach Number versus Shock Angle for 2D Wedge Domain

As is shown in Figure 12, the analytical model generated an accurate OSW position with small discrepancies likely resolvable with further mesh refinement. This gives credence to the following, inward-turning axisymmetric cases that were ran in comparison. It was also concluded that blockage ratio for the 2D flow field used did not make a noticeable impact on the OSW location due to of the lack of deviation from the analytical solution at any turning angle, inlet length, or Mach number.

Inward-Turning Axisymmetric Wedge Domain

The inward-turning axisymmetric cases yielded a Mach disk in the center at the coalescence point of all the OSWs. This is visualized in Figure 13 where a standing normal shock appears in the middle of the flow path. Like the non-axisymmetric case, all general flow features are in agreement with known supersonic, inviscid, ideal flow through a duct. When measured, the OSW

angle yielded steeper angles than that of the analytical solution. These results are plotted in Figure 14 where it is seen that as Mach number is decreased, the difference between analytical solution and observed results is more exaggerated.

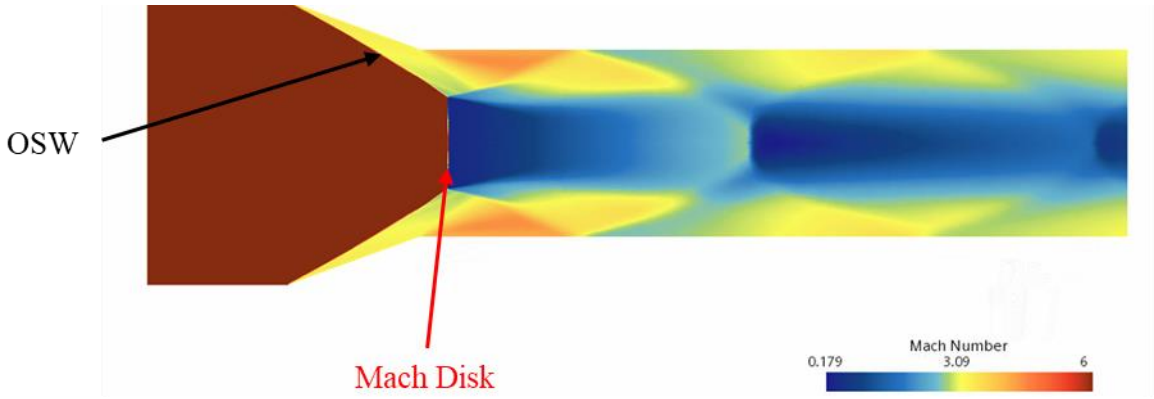

Figure 13: Mach Scalar Middle-Plane View of Axisymmetric Simulation with a 3 Inch Inlet Radius and $\theta = 20°$

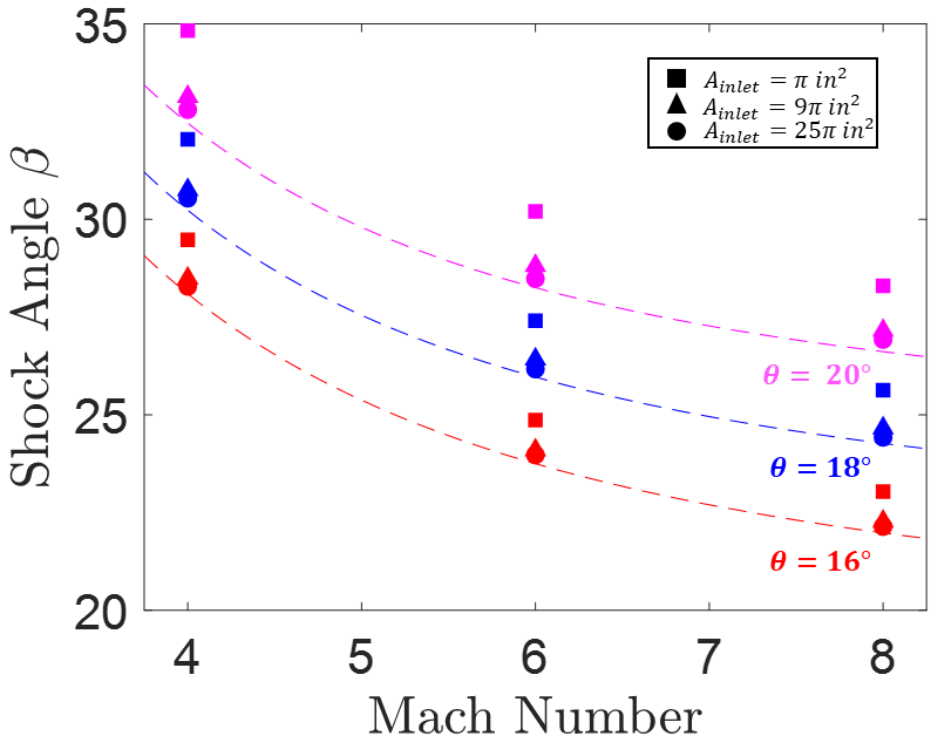

Figure 14: Mach Number versus Shock Angle for Inward-Turning Axisymmetric Flow

The blockage ratio from each axisymmetric case was then plotted against the difference in shock position normalized as a percent, which is shown in Figure 15. It was observed that the blockage ratio is proportional to the difference in analytical and realized OSW angles. In other words, the numerical solution tended to match the analytical prediction when the inner flow area was increased. This was expected because as the inlet radius increases, the penetration of the wedge becomes less significant, more closely resembling a finite 2D wedge.

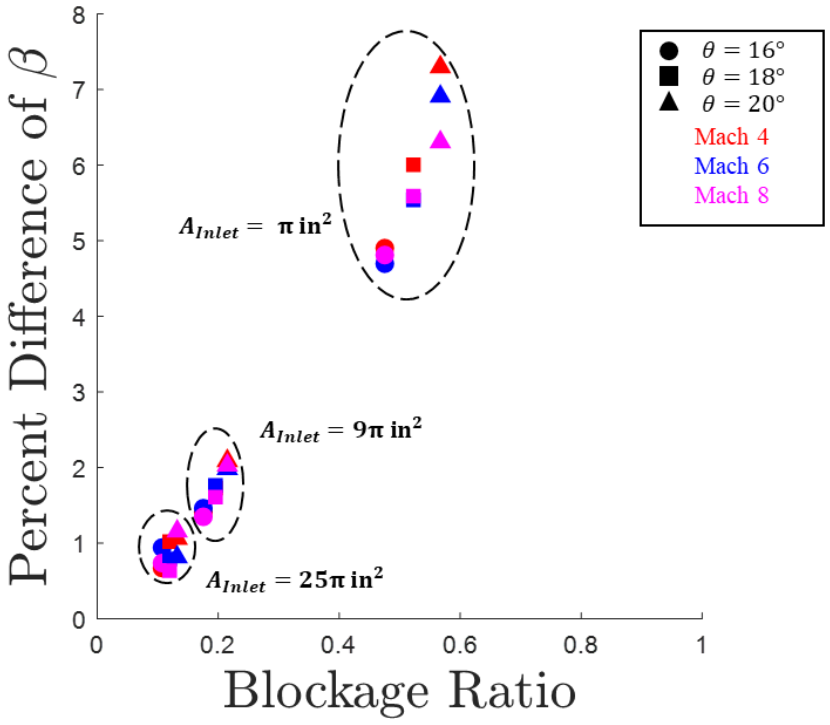

Figure 15: Blockage Ratio versus Percent Difference of β

CHAPTER 4: CONCLUSIONS

Most ODW research has focused on using an ODW anchored on a 2D wedge. An attractive alternative is a circular profile ODWE consisting of an inward-turning, axisymmetric flow path, which has generated a growing interest in studying its stability and performance. In such a configuration, the understanding of how the shock location of an OSW changes is limited. Understanding the physics of an OSW is vital to create an ODW shock polar, which characterizes the stability band of an ODW. This study numerically investigated the differences in the OSW location due to an inward-turning axisymmetric ODWE architecture to address this. Various wedge turning angles, inlet areas, and Mach numbers were examined to better characterize the changes in the OSW location as a function of these variables. The effect of the blockage ratio in the flow field was also examined to determine potential implications on the OSW location.

This research confirms that the OSW angle in such a flow was steeper than that of a numerical, 2D wedge simulation. For certain configurations, the OSW was found to be up to 8% steeper than what was analytically predicted. An increase in the blockage ratio also resulted in a higher percentage difference in the OSW location. This means that the steepening phenomenon became more pronounced as the flow was increasingly obstructed, resulting in the largest percent difference when the inlet was set to its smallest area.

Future work is most urgently needed to confirm the observed phenomenon in a viscous flow regime. It is unclear whether a viscous flow regime with a turbulence model will alter the position of an OSW in the architecture under inspection. It is also not clear how the presence of a boundary layer and potential recirculation zones will interact with the OSW in this configuration. Once this has been understood, a combustion model would need to be implemented to characterize the ODW

location further. Regardless, this work represents a fundamental step in helping build the foundation of knowledge required to design an inward-turning axisymmetric ODWE combustor. Paired with additional heat release from combustion, this work can potentially target the minimum entropy point of an ODW at a much shallower turning angle than previously thought in this configuration. This would allow inward-turning axisymmetric ODWE combustors to operate at a higher performance than their 2D-wedge counterparts while minimizing skin friction and integrating more seamlessly with conical inlet and isolator architectures. These benefits could enable inward-turning axisymmetric combustors to lead the next generation of hypersonic flight.

REFERENCES

[1] J. H. S. Lee, *The detonation phenomenon*. Cambridge University Press, 2008.

[2] D. T. Pratt, J. W. Humphrey, and D. E. Glenn, "Morphology of standing oblique detonation waves," *J Propuls Power*, vol. 7, no. 5, pp. 837–845, 1991, doi: 10.2514/3.23399.

[3] K. Kailasanath, "Review of propulsion applications of detonation waves," *AIAA journal*, vol. 38, no. 9, pp. 1698–1708, 2000, doi: 10.2514/2.1156.

[4] *Pulse Detonation Propulsion System-PEC Experience*. [Online]. Available: https://www.researchgate.net/publication/275653316

[5] W. H. Heiser and D. T. Pratt, *Hypersonic airbreathing propulsion*. American Institute of Aeronautics and Astronautics, 1994.

[6] C. Li, K. Kailasanath, and E. S. Oran, "Detonation structures behind oblique shocks," *Physics of Fluids*, vol. 6, no. 4, pp. 1600–1611, 1994, doi: 10.1063/1.868273.

[7] C. L. Bachman and G. B. Goodwin, "Ignition criteria and the effect of boundary layers on wedge-stabilized oblique detonation waves," 2020.

[8] S. A. Ashford and G. Emanuel, "Oblique detonation wave engine performance prediction," *J Propuls Power*, vol. 12, no. 2, pp. 322–327, 1996, doi: 10.2514/3.24031.

[9] D. Couture, A. Dechamplain, R. A. Stowe, P. G. Harris, W. H. C. Halswijk, and J. L. P. A. Moerel, "AIAA Senior Member 4 Research Scientist, Propulsion Group," 2008.

[10] J. Chan, J. P. Sislian, and D. Alexander, "Numerically simulated comparative performance of a scramjet and shcramjet at mach 11," *J Propuls Power*, vol. 26, no. 5, pp. 1125–1134, 2010, doi: 10.2514/1.48144.

[11] M. K. L. O'Neill and M. J. Lewis, "Design tradeoffs on scramjet engine integrated hypersonic waverider vehicles," *J Aircr*, vol. 30, no. 6, pp. 943–952, 1993, doi: 10.2514/3.46438.

[12] Q. Liu, D. Baccarella, and T. Lee, "Review of combustion stabilization for hypersonic airbreathing propulsion," *Progress in Aerospace Sciences*, vol. 119, Nov. 2020, doi: 10.1016/j.paerosci.2020.100636.

[13] C. L. Bachman and G. B. Goodwin, "Ignition criteria for oblique detonation waves in a hydrogen-air premixed freestream," in *AIAA Scitech 2021 Forum*, American Institute of Aeronautics and Astronautics Inc, AIAA, 2021, pp. 1–7. doi: 10.2514/6.2021-0688.

[14] "James E. John, Theo Keitch - Gas Dynamics-Pearson (2006)".

[15] R. Dudebout, J. P. Sislian, and R. Oppitz, “Numerical simulation of hypersonic shock-induced combustion ramjets,” *J Propuls Power*, vol. 14, no. 6, pp. 869–879, 1998, doi: 10.2514/2.5368.

[16] F. K. Lu, H. Fan, and D. R. Wilson, “Detonation waves induced by a confined wedge,” *Aerosp Sci Technol*, vol. 10, no. 8, pp. 679–685, Dec. 2006, doi: 10.1016/j.ast.2006.06.005.

[17] G. Xiang, Y. Zhang, X. Gao, H. Li, and X. Huang, “Oblique detonation waves induced by two symmetrical wedges in hydrogen-air mixtures,” *Fuel*, vol. 295, Jul. 2021, doi: 10.1016/j.fuel.2021.120615.

[18] H. Teng, H. D. Ng, and Z. Jiang, “Initiation characteristics of wedge-induced oblique detonation waves in a stoichiometric hydrogen-air mixture,” *Proceedings of the Combustion Institute*, vol. 36, no. 2, pp. 2735–2742, 2017, doi: 10.1016/j.proci.2016.09.025.

[19] G. Fusina, “Numerical Investigation of Oblique Detonation Waves for a Shcramjet Combustor,” 2003.

[20] G. Fusina, J. P. Sislian, and B. Parent, “Formation and stability of near chapman-jouguet standing oblique detonation waves,” *AIAA Journal*, vol. 43, no. 7, pp. 1591–1604, 2005, doi: 10.2514/1.9128.

[21] D. A. Rosato, M. Thornton, J. Sosa, C. Bachman, G. B. Goodwin, and K. A. Ahmed, “Stabilized detonation for hypersonic propulsion,” 2021, doi: 10.1073/pnas.2102244118/-/DCSupplemental.y.

[22] Y. Fang, Z. Zhang, and Z. Hu, “Effects of boundary layer on wedge-induced oblique detonation structures in hydrogen-air mixtures,” *Int J Hydrogen Energy*, vol. 44, no. 41, pp. 23429–23435, Aug. 2019, doi: 10.1016/j.ijhydene.2019.07.005.

[23] C. L. Bachman, G. B. Goodwin, and K. A. Ahmed, “Wedge-stabilized oblique detonation waves in a hypersonic hydrogen-air premixed freestream,” in *AIAA Propulsion and Energy Forum and Exposition, 2019*, American Institute of Aeronautics and Astronautics Inc, AIAA, 2019. doi: 10.2514/6.2019-4044.

[24] Z. P. White, M. R. Thornton, D. A. Rosato, A. R. Kotler, and K. A. Ahmed, “Experimental Study of Oblique Detonation Wave Stabilization on a Wedge,” American Institute of Aeronautics and Astronautics (AIAA), Jan. 2023. doi: 10.2514/6.2023-1497.

[25] M. Thornton, D. Rosato, and K. Ahmed, “Experimental Study of Oblique Detonation Waves with Varied Ramp Geometries,” in *AIAA Science and Technology Forum and Exposition, AIAA SciTech Forum 2022*, American Institute of Aeronautics and Astronautics Inc, AIAA, 2022. doi: 10.2514/6.2022-1753.